J Eng Math (2007) 57:133–144
DOI 10.1007/s10665-006-9119-1

ORIGINAL PAPER

An analytical solution for long-wave scattering by a submerged circular truncated shoal

Huan-Wen Liu · Yan-Bao Li

Received: 14 February 2005 / Accepted: 13 September 2006 / Published online: 25 November 2006

Abstract An analytical solution of the long-wave (or shallow-water) equation in closed-form is obtained for simple harmonic waves scattered by a submerged circular truncated shoal. This analytical solution is firstly validated against Longuet-Higgins's classical analytical solution for a submerged cylinder, and then validated against numerical solutions obtained by using the DRBEM (dual reciprocity boundary-element method) model for a submerged circular truncated cone. Finally, the analytical solution is used to investigate the changing trend of maximum wave amplification, the trace pattern of focal position of wave-energy versus the wave period and the influence of shoal submergence on wave-energy trapping.

Keywords Analytical solution · Long-wave equation · Shoal submergence · Submerged circular truncated shoal · Wave refraction and diffraction

1 Introduction

In a study on the phenomenon of wave refraction and diffraction, analytical solutions are to be favored over experimental data when they are used to verify numerical models; indeed, the accuracy of analytical solutions is only limited by the underlying assumptions and they are also more efficient than experimental data to reveal unknown physical phenomena. However, analytical solutions are, in general, only obtainable for simple bottom geometry or the simple wave equation. In linear wave theory, the mild-slope equation [1] has proved to be a very useful model for a wide range of water-wave problems; however, an exact analytical solution to it is still impossible as the wave-dispersion equation is implicit; even so, an approximate analytical solution has been recently presented in [2]. If we restrict our study to the linear long-wave equation, the problem becomes simpler and exact analytical solutions are possible.

In one dimension, Liu and Lin [3] and Lin and Liu [4] recently presented a closed-form analytical solution for wave interaction with a trench and an obstacle of general trapezoidal shape, which includes

H.-W. Liu
Faculty of Computer and Information Science, Guangxi University for Nationalities, Nanning, Guangxi 530006, P.R. China

Y.-B. Li (✉)
Department of Port and Coastal Engineering, Tianjin University, Tianjin 300072, P.R. China
e-mail: yanbao.li@263.net

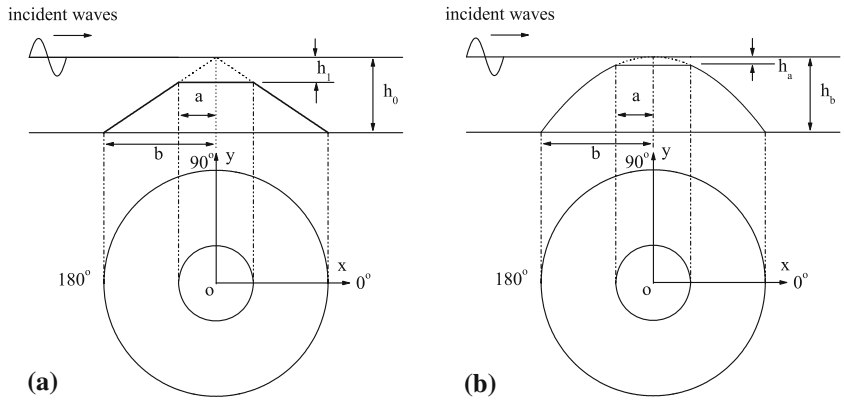

Fig. 1 A definition sketch of a submerged truncated shoal, where $h_1 = h_0 \frac{a^m}{b^m}$: (**a**) $m = 1$, (**b**) $m = 2$

several well-known analytical solutions as special cases, such as Lamb's classical solution [5] for waves passing over an infinitely long step, Mei's solution [6, pp. 130–134] for waves past a rectangular obstacle and Dean's solution [7] for an infinitely long shelf located behind a linear slope.

In two dimensions, several analytical solutions of the long-wave equation have been found for some axisymmetrical bottom geometries: for example, for a submerged cylinder [8], a cylindrical island mounted on a paraboloidal shoal [9], a conical island [10] and a cylindrical island mounted on a conical shoal [11]. Yu and Zhang [12] also derived a uniform form of the solutions to the long-wave equation for a cylindrical island mounted on an axisymmetrical shoal with different shapes. Kânoğlu and Synolakis [13] also solved the long-wave equation analytically for wave scattering by a conical island; however, their solution is actually an approximate solution, as the conical island is approximated by a series of sills in a stepwise fashion. Very recently, Suh et al. [14] derived an analytical solution for long waves propagating over a circular bowl pit.

In this paper, we seek an analytical solution of the long-wave equation for wave scattering by a submerged circular truncated shoal with the bottom geometry being an arbitrary power function (Fig. 1).

2 Solution technique

Consider the scattering of simple harmonic waves by a submerged circular truncated shoal, where a, b, h_1 and h_0 are the radius of the truncated plane, the radius of the toe, the water depth in the centre of the shoal and the constant water depth outside the shoal, respectively. Let x,y and z be Cartesian coordinates with origin located at the vertex of the un-truncated shoal on the still water level; then the water depth is given by

$$h(x,y) = h(r) = \begin{cases} h_1, & 0 \le r \le a, \\ \frac{h_0}{b^m} r^m, & a \le r \le b, \\ h_0, & r \ge b, \end{cases} \tag{1}$$

where $r = \sqrt{x^2 + y^2}$ and $h_1 : h_0 = a^m : b^m$.

According to the linear long-wave theory, the water elevation $\eta = \eta(x,y)$ satisfies the linear long-wave equation as follows:

$$\nabla \cdot (h \nabla \eta) + \frac{\omega^2}{g} \eta = 0, \tag{2}$$

in which $\nabla = (\partial/\partial x, \partial/\partial y)$, ω is the angular frequency and g the gravitational acceleration.

For harmonic waves, an incident wave with unit amplitude propagating along the positive x-axis can be expressed as

$$\eta_{inc} = \mathrm{e}^{\mathrm{i}k_0 x}, \tag{3}$$

where k_0 is the wave number related to the constant water depth h_0, i.e., $k_0 = \omega/\sqrt{gh_0}$. Since the topography is axisymmetric, we may introduce cylindrical coordinates (r, θ) with

$$\begin{cases} x = r\cos\theta, \\ y = r\sin\theta. \end{cases} \tag{4}$$

Under the new coordinates, Eq. 2 is transformed into

$$h\frac{\partial^2\eta}{\partial r^2} + \frac{\mathrm{d}h}{\mathrm{d}r}\frac{\partial\eta}{\partial r} + \frac{h}{r}\frac{\partial\eta}{\partial r} + \frac{h}{r^2}\frac{\partial^2\eta}{\partial\theta^2} + \frac{\omega^2}{g}\eta = 0. \tag{5}$$

By expanding η in Eq. 5 into a Fourier-cosine series as follows:

$$\eta(r,\theta) = \sum_{n=0}^{\infty} R_n(r)\cos n\theta, \quad (0 \le \theta \le 2\pi), \tag{6}$$

in which the integer n corresponds to solutions of different angular modes, and by using the technique of variable separation, the partial differential equation (5) can be transformed into an ordinary differential equation for each angular mode,

$$hr^2\frac{\mathrm{d}^2R_n(r)}{\mathrm{d}r^2} + \left[r^2\frac{\mathrm{d}h}{\mathrm{d}r} + hr\right]\frac{\mathrm{d}R_n(r)}{\mathrm{d}r} + \left[\frac{\omega^2}{g}r^2 - n^2h\right]R_n(r) = 0. \tag{7}$$

In the inner region with constant water depth h_1, Eq. 7 degenerates into a Bessel equation of the real order n:

$$r^2\frac{\mathrm{d}^2R_n(r)}{\mathrm{d}r^2} + r\frac{\mathrm{d}R_n(r)}{\mathrm{d}r} + \left[k_1^2r^2 - n^2\right]R_n(r) = 0, \tag{8}$$

which has, in general, two independent particular solutions $J_n(k_1r)$ and $Y_n(k_1r)$, where $J_n(k_1r)$ is the Bessel function of the first kind of order n and $Y_n(k_1r)$ is the Bessel function of the second kind of order n with k_1 being the local wave number with respect to the constant water depth h_1, i.e., $k_1 = \omega/\sqrt{gh_1}$. However, it is noted that $Y_n(k_1r)$ is singular at $r = 0$. Therefore, the general solution to Eq. 8 is just

$$R_n(r) = A_n^{(1)}J_n(k_1r), \tag{9}$$

and the water elevation in this region can be expressed as

$$\eta = \eta_1(r,\theta) = \sum_{n=0}^{\infty} A_n^{(1)}J_n(k_1r)\cos n\theta, \quad (r \le a, 0 \le \theta \le 2\pi), \tag{10}$$

in which, the constant coefficients $A_n^{(1)}$ are yet to be determined.

In the outer region with constant water depth h_0, Eq. 7 also degenerates into a Bessel equation of the real order n:

$$r^2\frac{\mathrm{d}^2R_n(r)}{\mathrm{d}r^2} + r\frac{\mathrm{d}R_n(r)}{\mathrm{d}r} + \left[k_0^2r^2 - n^2\right]R_n(r) = 0. \tag{11}$$

It is well-known that the water elevation may be written as [15]

$$\begin{aligned}\eta &= \eta_3(r,\theta) = \eta_{\mathrm{inc}}(r,\theta) + \eta_s(r,\theta) \\ &= \sum_{n=0}^{\infty}[\mathrm{i}^n\epsilon_nJ_n(k_0r) + A_n^{(4)}H_n^{(1)}(k_0r)]\cos n\theta, \quad (r \ge b, 0 \le \theta \le 2\pi),\end{aligned} \tag{12}$$

in which $H_n^{(1)}(k_0 r)$ is the Hankel function of the first kind of order n and the Jacobi symbols $\epsilon_n = 1$ for $n = 0$ and $\epsilon_n = 2$ for $n > 0$, respectively. In addition, the Sommerfeld far-field radiation condition has been used. The constant coefficients $A_n^{(4)}$ are also yet to be determined.

We now consider the region with variable water depth. By putting (1) into (7), we have

$$r^m \frac{\mathrm{d}^2 R_n}{\mathrm{d}r^2} + (m+1) r^{m-1} \frac{\mathrm{d}R_n}{\mathrm{d}r} + (\tau^2 - n^2 r^{m-2}) R_n = 0, \tag{13}$$

where $\tau = \omega\sqrt{b^m}/\sqrt{gh_0}$.

If $m = 2$, Eq. 13 becomes

$$r^2 \frac{\mathrm{d}^2 R_n}{\mathrm{d}r^2} + 3r \frac{\mathrm{d}R_n}{\mathrm{d}r} + (\tau^2 - n^2) R_n = 0, \tag{14}$$

which is the Euler equation. The general solution is known to be

$$R_n(r) = \begin{cases} A_n^{(2)} r^{-1} + A_n^{(3)} r^{-1} \log r, & \mu_n = 0, \\ A_n^{(2)} r^{\mu_n - 1} + A_n^{(3)} r^{-\mu_n - 1}, & \mu_n \neq 0, \end{cases} \tag{15}$$

with $\mu_n = \sqrt{n^2 + 1 - \tau^2}$. The coefficients $A_n^{(2)}$ and $A_n^{(3)}$ are to be determined.

If $m \neq 2$, we introduce the following transforms

$$t = c r^{1 - \frac{m}{2}}, \qquad \tilde{R}_n(t) = c^{\frac{m}{m-2}} t^{\frac{m}{2-m}} R_n\left(c^{\frac{2}{m-2}} t^{\frac{2}{2-m}}\right), \tag{16}$$

with $c = \frac{2\tau}{|2-m|}$. Note that

$$R_n(r) = c^{\frac{m}{2-m}} t^{\frac{m}{m-2}} \tilde{R}_n(t), \tag{17}$$

$$\frac{\mathrm{d}R_n(r)}{\mathrm{d}r} = \frac{2-m}{2} c^{\frac{m+2}{2-m}} t^{\frac{2m}{m-2}} \frac{\mathrm{d}\tilde{R}_n(t)}{\mathrm{d}t} - \frac{m}{2} c^{\frac{m+2}{2-m}} t^{\frac{m+2}{m-2}} \tilde{R}_n(t), \tag{18}$$

$$\begin{aligned} \frac{\mathrm{d}^2 R_n(r)}{\mathrm{d}r^2} = {} & \frac{(2-m)^2}{4} c^{\frac{m+4}{2-m}} t^{\frac{3m}{m-2}} \frac{\mathrm{d}^2 \tilde{R}_n(t)}{\mathrm{d}t^2} + \frac{3m(m-2)}{4} c^{\frac{m+4}{2-m}} t^{\frac{2m+2}{m-2}} \frac{\mathrm{d}\tilde{R}_n(t)}{\mathrm{d}t} \\ & + \frac{m(m+2)}{4} c^{\frac{m+4}{2-m}} t^{\frac{m+4}{m-2}} \tilde{R}_n(t), \end{aligned} \tag{19}$$

Equation 13 reads

$$t^2 \frac{\mathrm{d}^2 \tilde{R}_n}{\mathrm{d}t^2} + t \frac{\mathrm{d}\tilde{R}_n}{\mathrm{d}t} + (t^2 - \nu_n^2) \tilde{R}_n = 0, \tag{20}$$

with $\nu_n = \sqrt{4n^2 + m^2}/|2-m|$. Again, Eq. 20 is the Bessel equation of the real order ν_n and its general solution can be written as

$$\tilde{R}_n(t) = A_n^{(2)} J_{\nu_n}(t) + A_n^{(3)} Y_{\nu_n}(t). \tag{21}$$

The constant coefficients $A_n^{(2)}$ and $A_n^{(3)}$ are yet to be determined. From (6), (15), (16) and (21), the water elevation in this region can be written as

$$\eta_2(r,\theta) = \begin{cases} \sum_{n=0}^{\infty} \left[A_n^{(2)} r^{-1} + A_n^{(3)} r^{-1} \log r\right] \cos n\theta, & m = 2, \mu_n = 0, \\ \sum_{n=0}^{\infty} \left[A_n^{(2)} r^{\mu_n - 1} + A_n^{(3)} r^{-\mu_n - 1}\right] \cos n\theta, & m = 2, \mu_n \neq 0, \\ \sum_{n=0}^{\infty} r^{-\frac{m}{2}} \left[A_n^{(2)} J_{\nu_n}(c r^{1-\frac{m}{2}}) + A_n^{(3)} Y_{\nu_n}(c r^{1-\frac{m}{2}})\right] \cos n\theta, & m \neq 2. \end{cases} \tag{22}$$

The continuity of the wave elevations and the flow fluxes at $r = a$ and $r = b$ requires the following conditions

$$\eta_1(a,\theta) = \eta_2(a,\theta), \tag{23}$$

$$\frac{\partial \eta_1}{\partial r}(a,\theta) = \frac{\partial \eta_2}{\partial r}(a,\theta), \tag{24}$$

$$\eta_2(b,\theta) = \eta_3(b,\theta), \tag{25}$$

$$\frac{\partial \eta_2}{\partial r}(b,\theta) = \frac{\partial \eta_3}{\partial r}(b,\theta). \tag{26}$$

to be satisfied. Equivalently,

$$aJ_n(k_1a)A_n^{(1)} - A_n^{(2)} - \log a A_n^{(3)} = 0, \tag{27}$$
$$a^2k_1J_n'(k_1a)A_n^{(1)} + A_n^{(2)} + (\log a - 1)A_n^{(3)} = 0, \tag{28}$$
$$A_n^{(2)} + \log b A_n^{(3)} - bH_n^{(1)}(k_0b)A_n^{(4)} = b\mathrm{i}^n\epsilon_n J_n(k_0b), \tag{29}$$
$$A_n^{(2)} + (\log b - 1)A_n^{(3)} + b^2k_0H_n^{(1)'}(k_0b)A_n^{(4)} = -b^2k_0\mathrm{i}^n\epsilon_n J_n'(k_0b), \tag{30}$$

for $m = 2$ and $\mu_n = 0$, and

$$J_n(k_1a)A_n^{(1)} - a^{\mu_n-1}A_n^{(2)} - a^{-\mu_n-1}A_n^{(3)} = 0, \tag{31}$$
$$k_1J_n'(k_1a)A_n^{(1)} - (\mu_n - 1)a^{\mu_n-2}A_n^{(2)} + (\mu_n+1)a^{-\mu_n-2}A_n^{(3)} = 0, \tag{32}$$
$$b^{\mu_n-1}A_n^{(2)} + b^{-\mu_n-1}A_n^{(3)} - H_n^{(1)}(k_0b)A_n^{(4)} = \mathrm{i}^n\epsilon_n J_n(k_0b), \tag{33}$$
$$(\mu_n-1)b^{\mu_n-2}A_n^{(2)} - (\mu_n+1)b^{-\mu_n-2}A_n^{(3)} - k_0H_n^{(1)'}(k_0b)A_n^{(4)} = k_0\mathrm{i}^n\epsilon_n J_n'(k_0b), \tag{34}$$

for $m = 2$ and $\mu_n \neq 0$, and

$$J_n(k_1a)A_n^{(1)} - a^{-\frac{m}{2}}J_{\nu_n}(ca^{1-\frac{m}{2}})A_n^{(2)} - a^{-\frac{m}{2}}Y_{\nu_n}(ca^{1-\frac{m}{2}})A_n^{(3)} = 0, \tag{35}$$
$$k_1J_n'(k_1a)A_n^{(1)} + C_J(a)A_n^{(2)} + C_Y(a)A_n^{(3)} = 0, \tag{36}$$
$$b^{-\frac{m}{2}}J_{\nu_n}(cb^{1-\frac{m}{2}})A_n^{(2)} + b^{-\frac{m}{2}}Y_{\nu_n}(cb^{1-\frac{m}{2}})A_n^{(3)} - H_n^{(1)}(k_0b)A_n^{(4)} = \mathrm{i}^n\epsilon_n J_n(k_0b), \tag{37}$$
$$C_J(b)A_n^{(2)} + C_Y(b)A_n^{(3)} + k_0H_n^{(1)'}(k_0b)A_n^{(4)} = -k_0\mathrm{i}^n\epsilon_n J_n'(k_0b), \tag{38}$$

for $m \neq 2$, where

$$C_J(r) = \frac{m}{2}r^{-\frac{m+2}{2}}J_{\nu_n}(cr^{1-\frac{m}{2}}) + \frac{m-2}{2}cr^{-m}J_{\nu_n}'\left(cr^{1-\frac{m}{2}}\right), \tag{39}$$
$$C_Y(r) = \frac{m}{2}r^{-\frac{m+2}{2}}Y_{\nu_n}(cr^{1-\frac{m}{2}}) + \frac{m-2}{2}cr^{-m}Y_{\nu_n}'\left(cr^{1-\frac{m}{2}}\right). \tag{40}$$

By solving the system (27–30), all the four coefficients $A_n^{(1)}$, $A_n^{(2)}$, $A_n^{(3)}$ and $A_n^{(4)}$ can be determined as follows

$$A_n^{(i)} = D_i/D, \quad i = 1,\ldots,4, \tag{41}$$

where D_i and D are given below with respect to different cases:
(1) when $m = 2$, $\mu_n = 0$,

$$D_1 = \frac{2b^2\epsilon_n\mathrm{i}^{n+1}}{\pi},$$
$$D_2 = \frac{2ab^2\epsilon_n\mathrm{i}^{n+1}}{\pi}\left[J_n(k_1a)(1-\log a) - ak_1J_n'(k_1a)\log a\right],$$
$$D_3 = \frac{2ab^2\epsilon_n\mathrm{i}^{n+1}}{\pi}\left[J_n(k_1a) + ak_1J_n'(k_1a)\right],$$
$$D_4 = -a\epsilon_n\mathrm{i}^nJ_n(k_1a)\left[\left(1+\log\frac{b}{a}\right)b^2k_0J_n'(k_0b) + bJ_n(k_0b)\log\frac{b}{a}\right]$$
$$-a^2k_1\epsilon_n\mathrm{i}^nJ_n'(k_1a)\left[b^2k_0J_n'(k_0b)\log\frac{b}{a} + bJ_n(k_0b)\left(\log\frac{b}{a}-1\right)\right],$$
$$D = aJ_n(k_1a)\left[\left(1+\log\frac{b}{a}\right)b^2k_0H_n^{(1)'}(k_0b) + bH_n^{(1)}(k_0b)\log\frac{b}{a}\right]$$
$$+a^2k_1J_n'(k_1a)\left[b^2k_0H_n^{(1)'}(k_0b)\log\frac{b}{a} + bH_n^{(1)}(k_0b)\left(\log\frac{b}{a}-1\right)\right].$$

(2) when $m = 2$, $\mu_n \neq 0$,

$$D_1 = \frac{4\mu_n \mathrm{i}^n \epsilon_n}{\pi a^3 b},$$

$$D_2 = \frac{2\mathrm{i}^n \epsilon_n}{\pi b}\left[(\mu_n+1)a^{-\mu_n-2}J_n(k_1a) + k_1 a^{-\mu_n-1}J_n'(k_1a)\right],$$

$$D_3 = \frac{2\mathrm{i}^n \epsilon_n}{\pi b}\left[(\mu_n-1)a^{\mu_n-2}J_n(k_1a) - k_1 a^{\mu_n-1}J_n'(k_1a)\right],$$

$$\begin{aligned} D_4 = {} & -\mathrm{i}^n \epsilon_n k_0 J_n(k_1a)J_n'(k_0b)\left[(\mu_n-1)\,a^{\mu_n-2}b^{-\mu_n-1} + (\mu_n+1)\,a^{-\mu_n-2}b^{\mu_n-1}\right] \\ & - \mathrm{i}^n \epsilon_n (\mu_n^2-1) J_n(k_1a)J_n(k_0b)\left[a^{\mu_n-2}b^{-\mu_n-2} - a^{-\mu_n-2}b^{\mu_n-2}\right] \\ & + \mathrm{i}^n \epsilon_n k_1 k_0 J_n'(k_1a)J_n'(k_0b)\left[a^{\mu_n-1}b^{-\mu_n-1} - a^{-\mu_n-1}b^{\mu_n-1}\right] \\ & + \mathrm{i}^n \epsilon_n k_1 J_n'(k_1a)J_n(k_0b)\left[(\mu_n+1)a^{\mu_n-1}b^{-\mu_n-2} + (\mu_n-1)a^{-\mu_n-1}b^{\mu_n-2}\right], \end{aligned}$$

$$\begin{aligned} D = {} & k_0 J_n(k_1a)H_n^{(1)'}(k_0b)\left[(\mu_n-1)\,a^{\mu_n-2}b^{-\mu_n-1} + (\mu_n+1)\,a^{-\mu_n-2}b^{\mu_n-1}\right] \\ & + (\mu_n^2-1)J_n(k_1a)H_n^{(1)}(k_0b)\left[a^{\mu_n-2}b^{-\mu_n-2} - a^{-\mu_n-2}b^{\mu_n-2}\right] \\ & - k_1 k_0 J_n'(k_1a)H_n^{(1)'}(k_0b)\left[a^{\mu_n-1}b^{-\mu_n-1} - a^{-\mu_n-1}b^{\mu_n-1}\right] \\ & - k_1 J_n'(k_1a)H_n^{(1)}(k_0b)\left[(\mu_n+1)a^{\mu_n-1}b^{-\mu_n-2} + (\mu_n-1)a^{-\mu_n-1}b^{\mu_n-2}\right]. \end{aligned}$$

(3) when $m \neq 2$,

$$D_1 = \frac{2(m-2)\epsilon_n \mathrm{i}^{n+1}}{\pi^2 a^{m+1} b},$$

$$D_2 = \frac{2\epsilon_n \mathrm{i}^{n+1}}{\pi b}\left[C_Y(a)J_n(k_1a) + k_1 a^{-\frac{m}{2}}J_n'(k_1a)Y_{\nu_n}(ca^{1-\frac{m}{2}})\right],$$

$$D_3 = -\frac{2\epsilon_n \mathrm{i}^{n+1}}{\pi b}\left[C_J(a)J_n(k_1a) + k_1 a^{-\frac{m}{2}}J_n'(k_1a)J_{\nu_n}(ca^{1-\frac{m}{2}})\right],$$

$$\begin{aligned} D_4 = {} & \epsilon_n \mathrm{i}^n b^{-\frac{m}{2}} J_n(k_1a)\begin{vmatrix} C_J(a)Y_{\nu_n}\left(cb^{1-\frac{m}{2}}\right) - C_Y(a)J_{\nu_n}\left(cb^{1-\frac{m}{2}}\right) & b^{\frac{m}{2}}J_n(k_0b) \\ C_J(a)C_Y(b) - C_Y(a)C_J(b) & -k_0 J_n'(k_0b) \end{vmatrix} \\ & + \epsilon_n \mathrm{i}^n k_1 (ab)^{-\frac{m}{2}} J_n'(k_1a)\begin{vmatrix} J_{\nu_n}\left(ca^{1-\frac{m}{2}}\right)Y_{\nu_n}\left(cb^{1-\frac{m}{2}}\right) - Y_{\nu_n}\left(ca^{1-\frac{m}{2}}\right)J_{\nu_n}\left(cb^{1-\frac{m}{2}}\right) & b^{\frac{m}{2}}J_n(k_0b) \\ J_{\nu_n}\left(ca^{1-\frac{m}{2}}\right)C_Y(b) - Y_{\nu_n}\left(ca^{1-\frac{m}{2}}\right)C_J(b) & -k_0 J_n'(k_0b) \end{vmatrix}, \end{aligned}$$

$$\begin{aligned} D = {} & b^{-\frac{m}{2}} J_n(k_1a)\begin{vmatrix} C_J(a)Y_{\nu_n}\left(cb^{1-\frac{m}{2}}\right) - C_Y(a)J_{\nu_n}\left(cb^{1-\frac{m}{2}}\right) & -b^{\frac{m}{2}}H_n^{(1)}(k_0b) \\ C_J(a)C_Y(b) - C_Y(a)C_J(b) & k_0 H_n^{(1)'}(k_0b) \end{vmatrix} \\ & + k_1 (ab)^{-\frac{m}{2}} J_n'(k_1a)\begin{vmatrix} J_{\nu_n}\left(ca^{1-\frac{m}{2}}\right)Y_{\nu_n}\left(cb^{1-\frac{m}{2}}\right) - Y_{\nu_n}\left(ca^{1-\frac{m}{2}}\right)J_{\nu_n}\left(cb^{1-\frac{m}{2}}\right) & -b^{\frac{m}{2}}H_n^{(1)}(k_0b) \\ J_{\nu_n}\left(ca^{1-\frac{m}{2}}\right)C_Y(b) - Y_{\nu_n}\left(ca^{1-\frac{m}{2}}\right)C_J(b) & k_0 H_n^{(1)'}(k_0b) \end{vmatrix}. \end{aligned}$$

3 Results and discussion

3.1 Convergence of solution

The analytical solution presented in this paper is expressed as three infinite series (10), (12) and (22), which need to be truncated in a practical calculation, that is, a large enough integer N, which means the

total angular modes, need to be found such that these infinite series are approximated by finite series with the desired accuracy. Computational tests are conducted under the following geometrical parameters: $b = 10\,\text{m}, h_0 = 1\,\text{m}, h_1 = 0.5\,\text{m}, a = (h_1/h_0)^{\frac{1}{m}} b$. It is found that, when the wave amplification along a specific circle around the shoal is calculated, the shorter the incident waves are, the more the angular modes are needed. On the other hand, for the same incident wave, the further out the solutions are sought, the more the angular modes are needed, to obtain an accurate solution.

For example, for a shoal with power $m = 1$ and incident waves with period $T = 15$ s ($k_0 h_0 = 0.1338$), when we calculate the wave amplification along the circle $r = 2b$, 10 angular modes suffice to obtain convergent results with the absolute error being less than 0.5×10^{-6}. However, when we consider the wave amplification along the circle $r = 9b$, 25 angular modes have to be used to obtain accurate results. On the other hand, as the wave period is reduced to $T = 7$ s ($k_0 h_0 = 0.2867$), 15 angular modes have to be used to obtain convergent results with the same accuracy when we calculate the wave amplification along the circle $r = 2b$.

3.2 Verification

The current analytical model is firstly validated against the analytical solution by Longuet-Higgins for a submerged cylinder [8]. As shown in Fig. 2a, when we fix the parameters b, h_0, h_1 and let the power m increase, we can obtain a series of submerged circular truncated shoals which will approach a submerged cylinder. For $b = 10\,\text{m}, h_0 = 1\,\text{m}, h_1 = 0.5\,\text{m}$ and $m = 1, 2, 5, 10$ and 60, wave amplification along the x-axis is calculated and displayed in Fig. 2b. It can be seen that, as m increases, the current analytical solutions approach to Longuet-Higgins's analytical solution for a submerged cylinder [8].

Secondly, the current analytical model is validated against the numerical results by using the DRBEM (dual reciprocity boundary element method) model [16,17]. For convenience of comparison, we choose a submerged circular truncated cone (i.e., $m = 1$) with the following geometrical parameters: $a = 10\,\text{km}$, $b = 30\,\text{km}$, $h_0 = 4\,\text{km}$ and $h_1 = h_0/3$. To the authors' knowledge, the experimental data of wave amplification has never been reported before for this kind of submerged circular truncated cone. The wave amplifications along both the x-axis and the y-axis for the case of $T = 480\,\text{s}$ are calculated by using both the DRBEM model [16,17] and the present analytical model. The results are plotted in Fig. 3a, b. It is shown that the agreement between the two solutions is excellent along both the x- and y-axis.

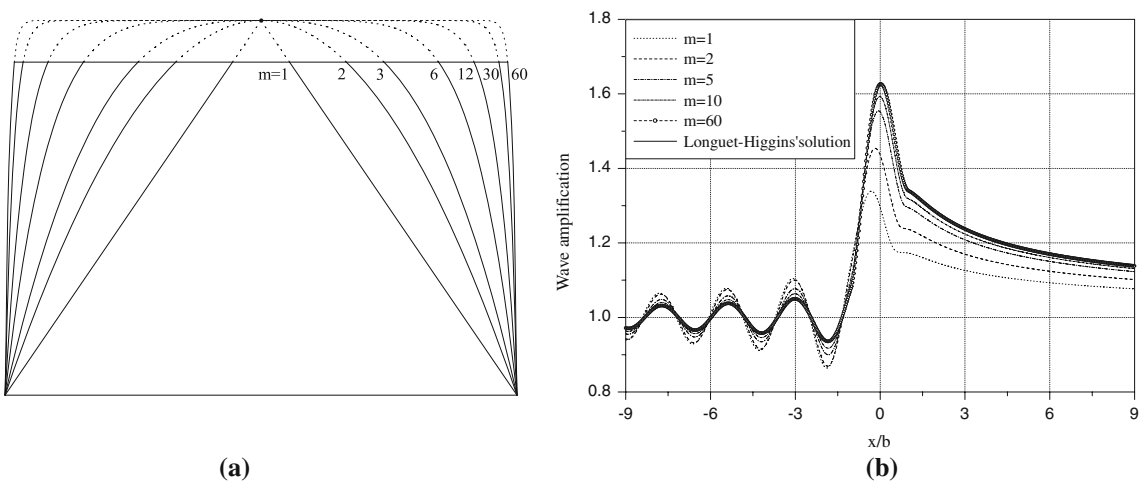

Fig. 2 (**a**) A series of submerged circular truncated shoals approximates a submerged cylinder; (**b**) comparison between the present solutions for submerged circular truncated shoals and Longuet-Higgins's solution for a submerged cylinder [8]

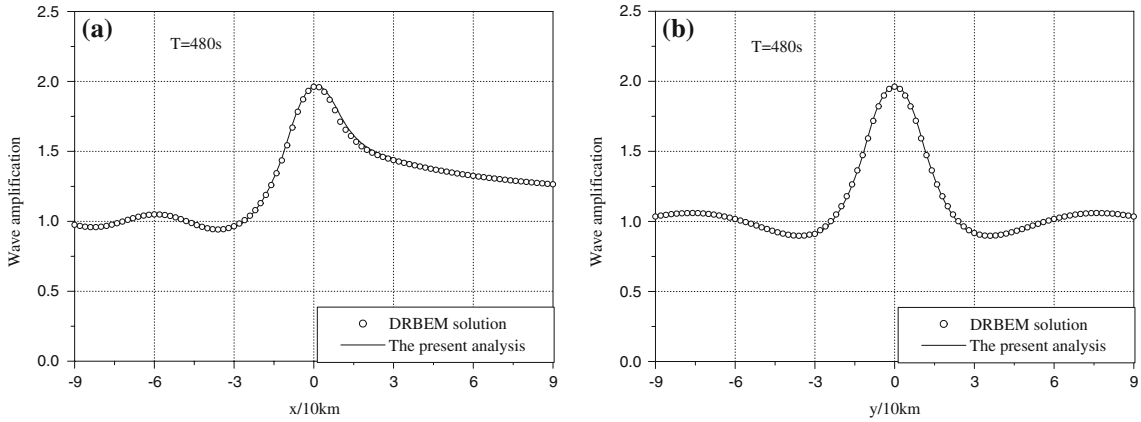

Fig. 3 Wave amplifications for a submerged circular truncated cone (i.e., $m = 1$) and for incident waves with $T = 480$ s, calculated by the DRBEM model [16,17] and by the present analytical model: (**a**) along the x-axis, (**b**) along the y-axis

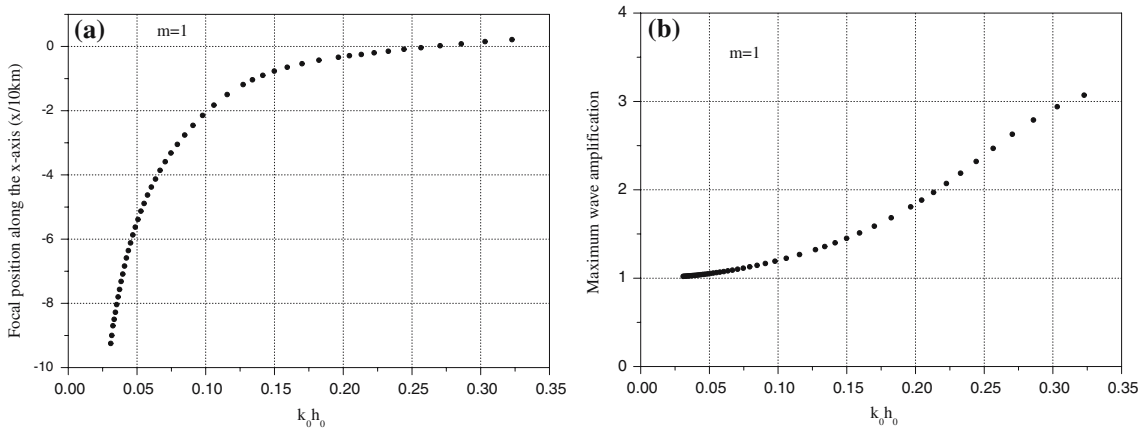

Fig. 4 The changing trend of (**a**): focal position and (**b**): maximum wave amplification along the x-axis, in the case of $m = 1$

3.3 Influence of wave period on scattering pattern

With the above validation of the current analytical model, we first investigate, for a fixed shoal submergence h_1/h_0, how the wave period would affect the wave scattering pattern. For $m = 1, 2, 3$, we choose the following geometrical parameters: $b = 30\,\text{km}$, $h_0 = 4\,\text{km}$, $h_1 = h_0/9$ and $a = (h_1/h_0)^{\frac{1}{m}}\, b$. We calculated the maximum wave amplifications along the x-axis for a large number of cases with the incident wave period ranging from 400 s ($k_0h_0 = 0.32279$) to 4100 s ($k_0h_0 = 0.03097$). When $m = 1$, it can be seen from Fig. 4a, b that both the focal position of wave energy and the maximum wave amplification are monotonic functions of k_0h_0; this means that, within the long-wave range, the focal point moves downstream and the maximum wave amplification increases with the decrease of incident wave period. This coincides with the refraction–diffraction theory for a submerged un-truncated shoal [18].

The case of $m = 2$ has also been studied by Lin and Liu [19], where, by employing an explicit Padé approximation to the implicit wave-dispersion relationship, an analytical solution to the approximated mild-slope equation in terms of series expansions was developed. Using their approximate analytical model, Lin and Liu investigated both the changing trend of the maximum wave amplification and the trace of the focal position of wave energy. It was observed that the maximum wave amplification is a multi-peak function, rather than a mono-peak function of k_0h_0; see Fig. 5b. In addition, when the period increases

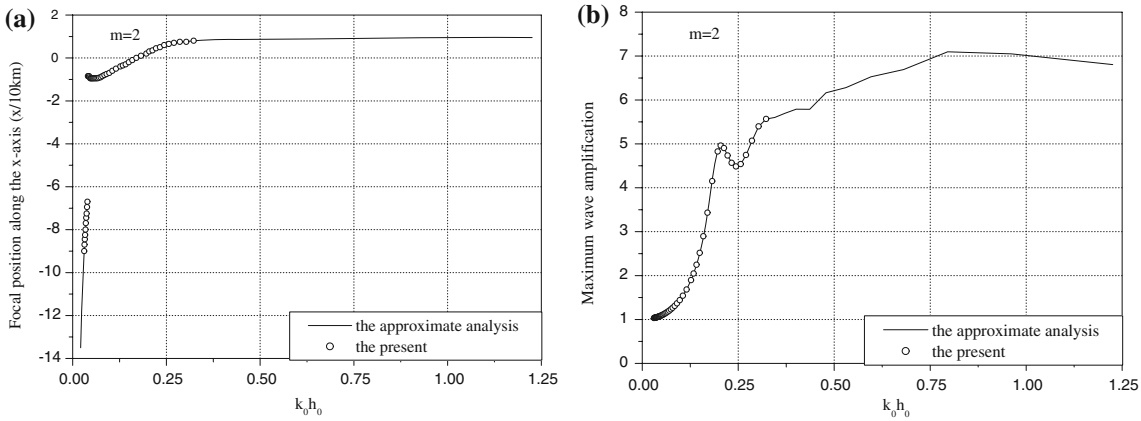

Fig. 5 The changing trend of (**a**): focal position and (**b**): maximum wave amplification along the x-axis, in the case of $m = 2$

from $T = 125\,\mathrm{s}$ ($k_0h_0 = 1.2255$) to $T = 2600\,\mathrm{s}$ ($k_0h_0 = 0.04884$), the focal point moves upstream from 9.5 km to −9.5 km; However, when the period further increases from $T = 2600$ s ($k_0h_0 = 0.04884$) to $T = 3100\,\mathrm{s}$ ($k_0h_0 = 0.04096$), the focal point moves back from −9.5 km to −8.5 km; and at $T = 3200$ s ($k_0h_0 = 0.03968$), the focal point abruptly jumps to −67 km and keeps moving upstream again with an increase of wave period; see Fig. 5a. This exceptional trace pattern of the focal position is different from the experimental data for a submerged un-truncated paraboloidal shoal [18] and has never been reported before to the authors' knowledge. However, since this observation is based on the results obtained by the approximate model, rather than by an exact analytical model, it is necessary to be re-examined here by using the current analytical model. A large number of cases with wave period ranging from 400 s ($k_0h_0 = 0.32279$) to 4100 s ($k_0h_0 = 0.03097$) are tested and compared with Lin and Liu's approximate analytical solutions; see Fig. 5a, b. As we can see, the agreement between two groups of solutions is very good within the long-wave range, and therefore the exceptional phenomenon revealed by Lin and Liu [19] is confirmed.

A similar phenomenon can be also observed in the case of $m = 3$. As shown in Fig. 6a, when the period increases from $T = 400\,\mathrm{s}$ ($k_0h_0 = 0.32279$) to $T = 2200\,\mathrm{s}$ ($k_0h_0 = 0.05773$), the focal point moves upstream from 11.2 km to −7.05 km; however, when the period further increases from $T = 2200\,\mathrm{s}$ ($k_0h_0 = 0.05773$) to $T = 4100\,\mathrm{s}$ ($k_0h_0 = 0.03097$), the focal point moves back from −7.05 km to −4.8 km. In addition, as

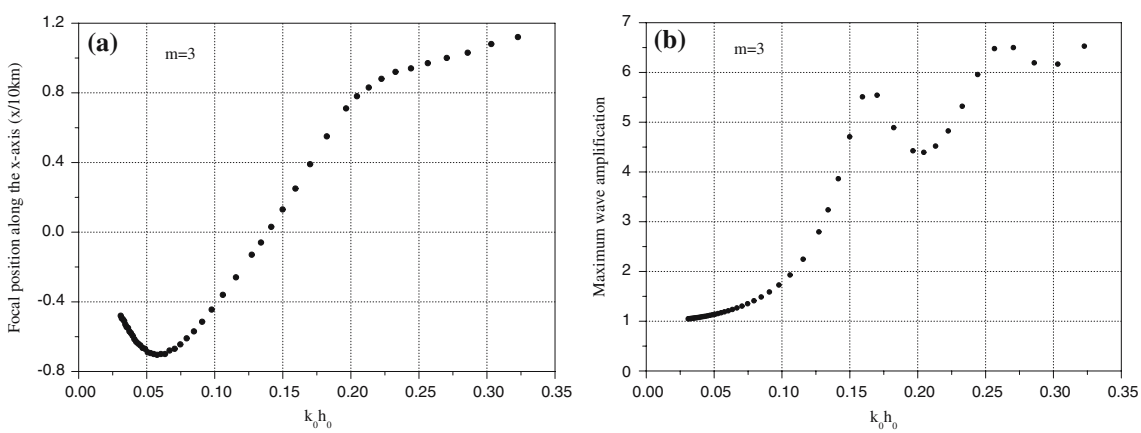

Fig. 6 The changing trend of (**a**): focal position and (**b**): maximum wave amplification along the x-axis, in the case of $m = 3$

we can see from Fig. 6b, the maximum wave amplification is also a multi-peak function, rather than a mono-peak function of k_0h_0.

3.4 Influence of shoal submergence on scattering pattern

For a given incident wave, we look into the influence of the shoal submergence h_1/h_0 on the wave-scattering pattern. For four incident waves with their period being 900, 720, 600 and 480 s, respectively, we fix $b = 30$ km and $h_0 = 4$ km; some values of h_1/h_0, which vary from 0.99 to 0.05, are tested for both the conical shoal ($m = 1$) and the paraboloidal shoal ($m = 2$).

When $m = 1$, it is seen from Figs. 7–8 that, for the largest values of h_1/h_0 (e.g. 0.99 and 0.75, deep submergence), the wave amplification is weak, as expected. As the shoal height increases ($h_1/h_0 = 0.50$ and 0.25), the maximum value of amplification becomes larger. When $h_1/h_0 = 0.10$, the amplification further increases. If the shoal height further increases to the ratio $h_1/h_0 = 0.05$, the amplifications reach 1.41 (at $x = -8$ km), 1.67 (at $x = -3$ km), 2.04 (at $x = -2$ km) and 2.78 (at $x = 0$ km), respectively. A similar changing trend of the maximum wave amplification versus the shoal submergence is observed for $m = 2$.

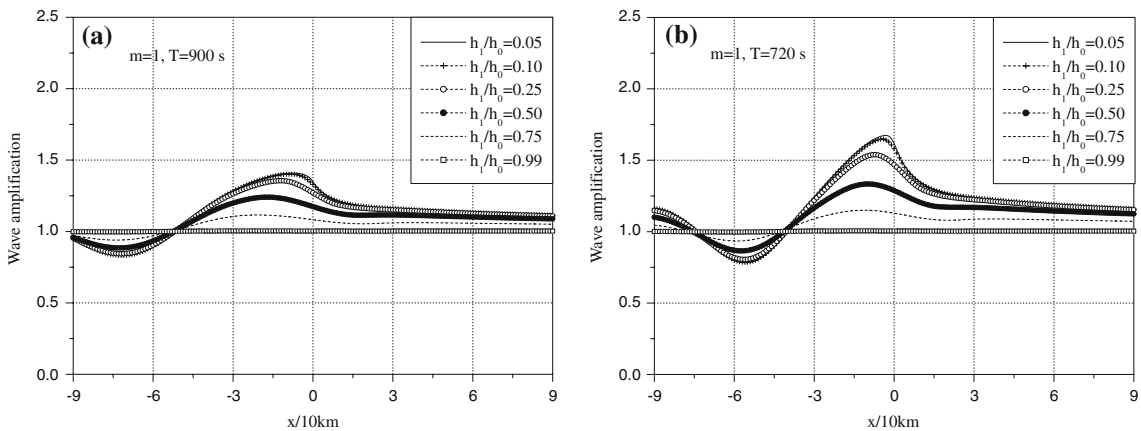

Fig. 7 Wave amplification along the x-axis for incident waves $T = 900$ and 720 s with various shoal submergences

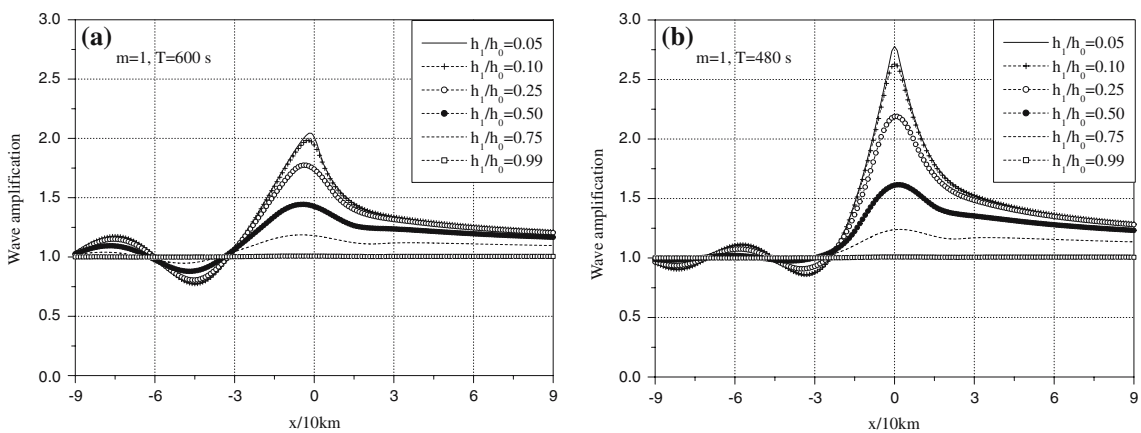

Fig. 8 Wave amplification along the x-axis for incident waves $T = 600$ and 480 s with various shoal submergences

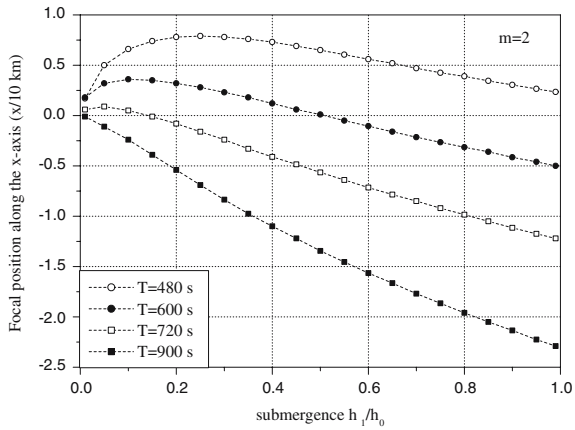

Fig. 9 The changing trend of focal position along the x-axis versus the shoal submergence h_1/h_0 in the case of $m = 2$

As for the location of the focal point, when $m = 1$, it is interesting to observe that, for the three cases with $T = 900$ s, $T = 720$ s and $T = 600$ s, the focal points move downstream with a decrease of the shoal submergence; however, for the other case with $T = 480$ s, the focal points move upstream for decreasing shoal submergence. When $m = 2$, the focal position along the x-axis versus the shoal submergence h_1/h_0 is plotted in Fig. 9. It is shown that, for relatively short waves (e.g., $T = 480$, 600 and 720 s), the focal point moves downstream first and then moves upstream for increasing shoal submergence. And for relatively long waves (e.g., $T = 900$ s), the focal point moves upstream when the shoal submergence increases and the distance of the focal point to the shoal centre is almost linearly proportional to h_1/h_0. It is found that the focal position always moves towards the shoal centre with a reduction of the shoal submergence.

4 Conclusion

In this study, an analytical technique is developed for solving the linear long-wave equation for water-wave refraction and diffraction above a submerged circular truncated shoal. In particular, this approach is used in this study to examine wave-energy trapping by a submerged shoal.

For a particular shoal submergence of h_1/h_0, it is found from the analysis of the analytical results that, when $m = 1$, wave amplification increases and the focus point shifts downstream with a wave period decrease within the long-wave range. When $m = 2$ and $m = 3$, the maximum wave amplification is a multi-peak, rather than a mono-peak function of k_0h_0. When $m = 3$, the focal point moves upstream for very long waves and then moves back when the wave period is increased. When $m = 2$, the trace pattern of the focal position revealed by Lin and Liu [19], using an approximate analytical solution to the mild-slope equation, is confirmed by our exact analytical solution.

For a particular incident wave, however, the maximal wave amplitude keeps increasing as the local water depth above the shoal centre, which is characterized by h_1/h_0, decreases. The focal point moves towards the shoal centre for a reduction of h_1/h_0, although it may shift from either the upstream side or the downstream side.

Acknowledgements The first author would like to gratefully acknowledge support from the National Science Foundation of China (10162001, 10462001), the Special Funding for Returning Overseas Scholars of China State Education Ministry (2005-55), the Shi-Bai-Qian Talents Program in Guangxi (2001224), the Natural Science Foundation in Guangxi (0575029, 0639008) and a Research Project in Guangxi Education Department. Their thanks are also given to anonymous referees for their valuable suggestions.

References

1. Smith R, Sprinks T (1975) Scattering of surface waves by a conical island. J Fluid Mech 72:373–384
2. Liu H-W, Lin P-Z, Shankar NJ (2004) An analytic solution for combined refraction and diffraction based on the mild-slope equation. Coastal Engng 51:421–437
3. Liu H-W, Lin P-Z (2005) Discussion of "Wave transformation by two-dimensional bathymetric anomalies with sloped transitions" [Coast. Eng. 50 (2003) 61–84]. Coastal Engng 52:197–200
4. Lin P-Z, Liu H-W (2005) Analytical study of linear long-wave reflection by a two-dimensional obstacle of general trapezoidal shape. J Engng Mech 131:822–830
5. Lamb H (1932) Hydrodynamics, 6th edn. Dover
6. Mei CC (1989) The applied dynamics of ocean surface waves. World Scientific, Singapore
7. Dean RG (1964) Long wave modification by linear transitions. J Waterways Harbors Div, Proc ASCE 90(WW1)1–29
8. Longuet-Higgins MS (1967) On the trapping of wave energy round islands. J Fluid Mech 29:781–821
9. Homma S (1950) On the behaviour of seismic sea waves around circular island. Geophys Mag 21:199–208
10. Zhang YL, Zhu, S-P. (1994) New solutions for the propagation of long water waves over variable depth. J Fluid Mech 278:391–406
11. Zhu S-P, Zhang YL (1996) Scattering of long waves around a circular island mounted on a conical shoal. Wave Motion 23:353–362
12. Yu XP, Zhang BY (2003) An extended analytic solution for combined refraction and diffraction of long waves over circular shoals. Ocean Engng 30:1253–1267
13. Kânoğlu U, Synolakis CE (1998) Long wave runup on piecewise linear topographies. J Fluid Mech 374:1–28
14. Suh K-D, Jung T-H, Haller MC (2005) Long waves propagating over a circular bowl pit. Wave Motion 42:143–154
15. MacCamy RC, Fuchs RA (1954) Wave forces on piles: a diffraction theory. US Army Corps of Engineering, Beach Erosion Board, Washington, DC, Tech. Mem. 69
16. Liu H-W (2001) Numerical modeling of the propagation of ocean waves. Ph.D. Thesis, University of Wollongong, Australia
17. Zhu S-P, Liu H-W, Chen K (2000) A general DRBEM model for wave refraction and diffraction. Engng Anal Boundary Elements 24:377–390
18. Suh KD, Lee C, Park YH, Lee TH (2001) Experimental verification of horizontal two-dimensional modified mild-slope equation model. Coastal Engng 44:1–12
19. Lin P-Z, Liu H-W Scattering and trapping of wave energy by a submerged truncated paraboloidal shoal. J Waterway, Port, Coast Ocean Engng (to appear)